Published in Journal of Lightwave Technology 22, issue 10, 2323-2332, 2004
which should be used for any reference to this work

Absorption and Light Scattering in InGaN-on-Sapphire- and AlGaInP-Based Light-Emitting Diodes

Sven-Silvius Schad, Barbara Neubert, Christoph Eichler, Marcus Scherer, Frank Habel, Matthias Seyboth, Ferdinand Scholz, Daniel Hofstetter, Peter Unger, *Member, IEEE*, Wolfgang Schmid, Christian Karnutsch, and Klaus Streubel

***Abstract*—Different experimental and simulation techniques aiming at a better understanding of lateral mode absorption in light-emitting diodes (LEDs) are presented in this paper. A measurement of transmitted power versus propagation distance allows us to derive the absorption losses of LED layer structures at their emission wavelength. Two models for the observed intensity distribution are presented: one is based on scattering, whereas the other relies on selective absorption. Both models were applied to InGaN-on-sapphire-based LED structures. Material absorption losses of 7 cm^{-1} for the scattering model and 4 cm^{-1} for the absorbing-layer model were obtained. Furthermore, these values are independent of the emission wavelength of the layer structure in the 403–433-nm range. The losses are most likely caused by a thin highly absorbing layer at the interface to the substrate. In a second step, interference of the modal field profile with the absorbing layer can be used to determine its thickness ($d = 75$ nm) and its absorption coefficient ($\alpha \approx 3900$ cm^{-1}). This method has also been tested and applied on AlGaInP-based layer structures emitting at 650 nm. In this case, the intensity decay of $\alpha = 30$ cm^{-1} includes a contribution from the absorbing substrate.**

***Index Terms*—Absorption, AlGaInP, buffer absorption, buffer scattering, InGaN, light-emitting diodes (LEDs), nucleation.**

I. Introduction

THE HIGH PERFORMANCE of state-of-the-art light-emitting diodes (LEDs) has opened a whole range of new applications such as traffic signals, automotive rear lights, and large-area full-color outdoor displays. Besides improvement of epitaxial methods and device processing, the problem of light extraction became a further important field of research. The occurrence of total internal reflection and absorption causes a significant fraction of light to remain trapped in the semiconductor and become lost. In order to overcome the problem of total internal reflection, different strategies leading to novel chip designs were proposed.

In resonant-cavity (RC) LEDs, the internal radiation pattern is changed by coupling to a resonator. An improvement of light extraction is achieved by increasing the fraction of light propagating perpendicular to the surface. Further improvement could be obtained by outcoupling of remaining guided modes using photonic crystals [1]. Scattering at the semiconductor surface is aimed in surface-textured thin-film LEDs [2]. The extraction enhancement is achieved by scattering of the internally reflected light at the textured surface. These scattering processes change the propagation angle of nonescaping photons. Together with a highly reflective mirrorlike bottom surface, multiple scattering events are possible, and extraction gets more likely every time the surface is hit.

Besides modification of the spontaneous emission behavior and statistical light extraction approaches, a change in chip geometry is another promising strategy. The most efficient one regarding extraction is the use of truncated inverted pyramids (TIPs) [3], [4]. It uses a structured thick window layer that serves as reflector. Most of the light is extracted through the top surface, whereas the reflected part escapes through the sidewalls. Yet another chip design is implemented in the tapered LED. The light is generated in the center of a circularly symmetric device and is guided to a tapered region. Within the latter, the angle of incidence is reduced at every reflection until extraction of the guided modes takes place.

Losses can significantly reduce the device efficiency, therefore they have a major impact on the success of an extraction approach. For optimization, the different loss mechanisms have to be identified and quantified. Thus, the scope of this paper is to address light scattering, absorption, and its distribution.

II. Measurement Method

As opposed to established measurement methods, we employ a fully integrated optical waveguide experiment that is fabricated using standard processing techniques (see Fig. 1). For the determination of absorption losses, intensity versus propagation distance in the material is measured. This is achieved by an arrangement of an electrically passive waveguide (100-μm width) and two electrically active rectangular LED structures (20×100 μm^2) in a unit. The aim of the two rectangular LEDs

S.-S. Schad, B. Neubert, C. Eichler, M. Scherer, F. Habel, M. Seyboth, F. Scholz, P. Unger are with the Department of Optoelectronics, University of Ulm, D-89069 Ulm, Germany.

D. Hofstetter is with the University of Neuchatel, 2000 Neuchatel, Switzerland.

W. Schmid was with the Department of Optoelectronics, University of Ulm, D-89069 Ulm, Germany. He is now with OSRAM Opto Semiconductors, 93049 Regensburg, Germany.

C. Karnutsch was with OSRAM Opto Semiconductors, 93049 Regensburg, Germany. He is now with Light Technic Institute, University of Karlsruhe, 76131 Karlsruhe, Germany.

K. Streubel is with OSRAM Opto Semiconductors, 93049 Regensburg, Germany.

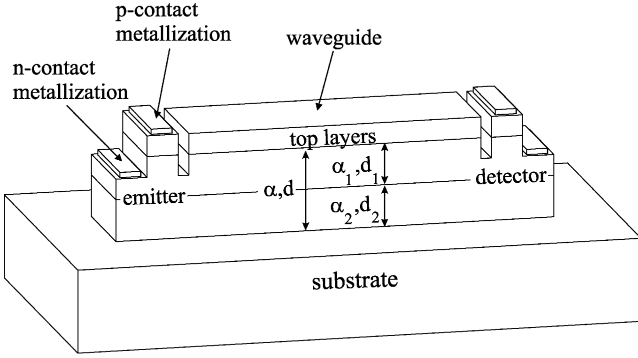

Fig. 1. Arrangement of emitting LED, waveguide, and detector LED used for PMM.

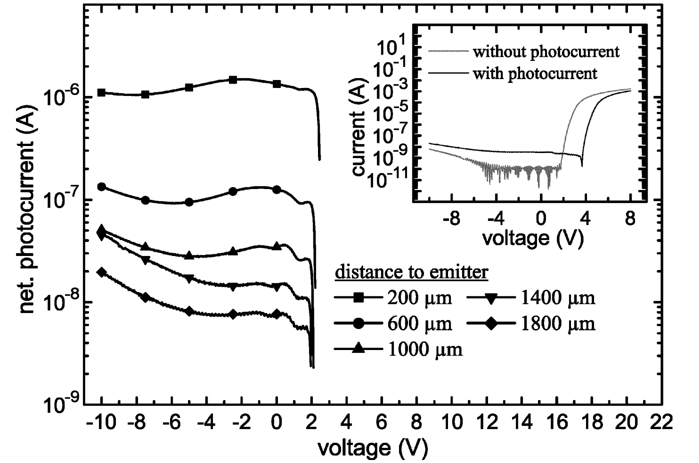

Fig. 2. Measured photocurrent in dependence of distance for a typical set of InGaN waveguides. Inset depicts I–V curve of a detector LED with and without photocurrent.

is to serve as an excitation source and as a detector, respectively. The active LED structures are located at the front and back end of the waveguide region. Electrical isolation between active and passive sections is accomplished by etching 2-μm-deep grooves across the waveguide. The LED structure for excitation is driven at forward current, whereas at the detecting structure, a negative bias is applied, and the photocurrent is measured. Thus, the method is named the photocurrent measurement method (PMM). To obtain an intensity distribution as a function of distance, different units having waveguide lengths between 200 and 3000 μm are necessary. Each unit provides one data point for a specific distance as explained subsequently. The mesa formation is accomplished by a dry-etching process. Thus, steep sidewalls down to the substrate enable a lateral guiding by the semiconductor–air interface over the whole epitaxial stack.

For each unit, the same current is applied to the emitting LED structure, and the photocurrent is measured at the dedicated detecting LED structure. One advantage of an integrated optical experiment is the self-alignment of emitter, waveguide, and detector by the mask design. This provides the same coupling coefficients from emitter to waveguide as well as from waveguide to the detector for each unit. The relatively large groove of 4 μm width between the emitter, waveguide, and detector will introduce large coupling losses. However, because of the much larger lateral dimension, enough light remains in the system to obtain a sufficient photocurrent.

Thus, the intensity distribution in an undisturbed waveguide can be determined. Furthermore, a sufficiently homogeneous epitaxy regarding the emission wavelength and the output power of the emitters is assumed. Since the structure is used for detection, a spectrally resolved behavior cannot be obtained. In addition, a spectral weighting due to the sensitivity of the LED detector possibly has to be accepted. Since coupling of spontaneous emitted light into a single-mode waveguide is inefficient, a multimode waveguide has to be used for this kind of experiment, and therefore, waveguide dispersion is considered for the evaluation of the intensity distribution (see Section IV-A).

The wave guiding in the vertical direction depends on the investigated material system and the layer structure itself. Regarding group III nitrides grown on sapphire, total internal reflection at the GaN–air interface and the GaN–sapphire interface occur for modes with effective index between the refractive index of GaN and the refractive index of the substrate. For AlGaInP-based devices grown on GaAs, no total internal reflection exists at the substrate–epi interface. However, the large extinction coefficient causes an exponential intensity decay, which can be regarded as a weak node for the electric and magnetic field. Thus, a contribution of the substrate absorption to the overall lateral intensity decay is given.

III. EXPERIMENTAL

The measurements are done using a HP4145 semiconductor parameter analyzer. I–V curves of the detector LED structures are shown in the inset of Fig. 2 with and without illumination for InGaN-on-sapphire structures. First, we discuss the dark current I–V curves of the detector structures without illumination. Toward large negative voltages, the current arises. This behavior can be modeled by a resistor in parallel to an ideal p–n-junction. Since we have observed a clear dependence on the length of the mesa edge from the analysis of different geometries (not shown), we assume that etching-induced defects are the origin of this anomal current increase. Between -5 and 1.7 V, the current wiggles because of the noise limit of the semiconductor parameter analyzer.

Applying an emitter forward current of 10 mA causes a significant increase in the detector current. The induced photocurrent acts as a current source in the detecting LED structure and a self-biasing occurs. Thus, a virtual increase in forward voltage V_f is observed. To get rid of the parasitic leakage current and the noise current, a subtraction of both curves is performed. Thus, Fig. 2 depicts the absolute value of the net photocurrent. However, for low currents and large reverse biases, an influence of leakage current remains. Furthermore, the photocurrent is a function of voltage, since a band alignment due to the quantum-confined Stark effect occurs. Around $V = 0$, however, the I–V curves are alike for different excitations, and the photocurrent is free of parasitic effects.

We investigated three InGaN-on-sapphire samples (S1–S3). They have been grown using the same growth parameters with respect to the nucleation, recrystallization, and the further

TABLE I

LAYER STRUCTURE USED FOR THE CALCULATION OF MODAL ABSORPTION COEFFICIENTS FOR A HOMOGENOUS LAYER ABSORPTION DISTRIBUTION (SEE FIG. 1). THE REFRACTIVE INDEX WAS TAKEN FROM LITERATURE [8] FOR A WAVELENGTH OF $\lambda = 400$ nm

	thickness (nm)	material	n	α
top layers	250	p-GaN:Mg	2.5410	
	20	$Al_{0.3}Ga_{0.7}N$:Mg	2.3847	
	5	GaN	2.5410	α_1
	5x { 4	InGaN	2.5410	
	5x { 5	GaN	2.5410	
	$d = d_1 = 1500$	n-GaN:Si	2.5410	α_1
	300000	sapphire	1.7866	0

TABLE II

LAYER STRUCTURE USED FOR THE CALCULATION OF MODAL ABSORPTION COEFFICIENTS IF A BOTTOM-LAYER ABSORPTION IS ASSUMED (SEE FIG. 1). d_2 DENOTES THE THICKNESS OF THE ABSORBING LAYER, AND $d_1 + d_2 = 1500$

	thickness (nm)	material	n	α
top layers	250	p-GaN:Mg	2.5410	
	20	$Al_{0.3}Ga_{0.7}N$:Mg	2.3847	
	5	GaN	2.5410	0
	5x { 4	InGaN	2.5410	
	5x { 5	GaN	2.5410	
	$d = 1500$ { d_1	n-GaN:Si	2.5410	α_1
	$d = 1500$ { d_2	absorbing GaN	2.5410	α_2
	300000	sapphire	1.7866	0

growth. Only the quantum-well thickness has been adjusted. The layer structure is as follows (see Tables I and II). On a sapphire substrate with a thickness of about 300 μm, a nucleation layer of about 30 nm is employed and an approximately 1.5-μm buffer layer is grown. During the growth, Si doping has been applied ($n = 2 \cdot 10^{18}$ cm^{-3}). The next layers form a multiple-quantum-well (MQW) structure with five compressively strained well/barrier pairs followed by an approximately 10-nm-thick AlGaN barrier containing approximately 30% aluminum. The final top layer is Mg-doped GaN with a thickness of 250 nm ($p = 4 \cdot 10^{17}$ cm^{-3}). The emission wavelength was adjusted by the thickness of the wells; thus, a shift of the ground level of the quantum wells was preferred over a variation of their indium content. The three samples exhibit emission wavelengths of 404, 431, and 433 nm and show output powers larger than 1 mW at a current of 20 mA for on-wafer devices. The obtained intensity versus distance behavior is depicted in Fig. 3. The dependence is clearly nonexponential, and despite different emission wavelengths, the samples exhibit nearly the same distance dependence. As reported previously, the intensity distribution is not affected by the common rough backsurface of the sapphire substrate [5]. Due to the quantum-confined Stark effect, the absorption edge of the wells is detuned toward higher energies with respect to the emission photon energy [5]. Thus, absorption properties of bulk GaN are governing the absorption properties at the emission wavelength. The intensity distribution is caused by a complex interplay between waveguide dispersion, scattering, and material absorption and will be discussed subsequently.

A similar intensity distribution can be observed on AlGaInP-based LED structures. We will briefly outline the layer structure of an AlGaInP-based sample, show the experimental intensity distribution, and discuss the results.

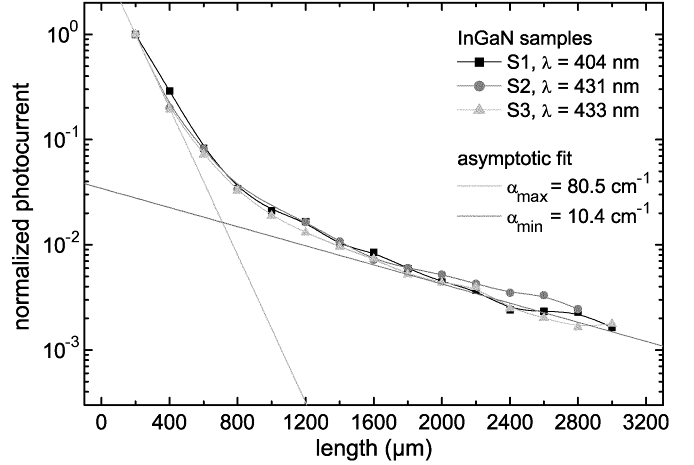

Fig. 3. Photocurrent versus distance for the three InGaN-LED structures with emission 404, 431, and 433 nm.

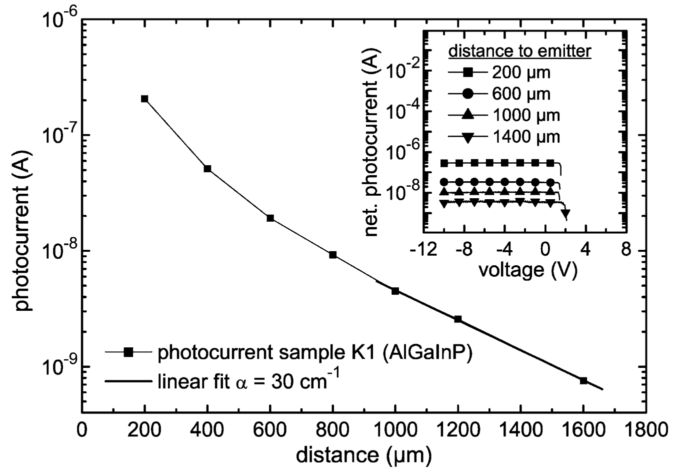

Fig. 4. Sample K1: Intensity distribution for AlGaInP-based LED structures with an emission wavelength of $\lambda = 650$ nm. Data is fit by an exponential law above 900 μm, $\alpha = 30$ cm^{-1}. The inset depicts the net photocurrent.

The active region consists of three compressively strained InGaP/AlGaInP quantum wells, which are sandwiched between two InAlP confinement layers. On the n-side of the p–n-junction, a 3.1-μm $Al_{0.6}Ga_{0.4}As$ follows, whereas on the p-side, a 420-nm-thick $Al_{0.6}Ga_{0.4}As$ layer is grown. The inset of Fig. 4 shows the photocurrent versus bias for the sample K1 emitting at 650 nm. A current of 5 mA was applied to the emitting structure. In contrast to the nitride samples, no voltage dependence is obtained. A similar evaluation of the IV curves yields the intensity distribution, which is depicted in Fig. 4. Apart from the first 900 μm, the intensity decay is exponential. A linear fit leads to an intensity decay of $\alpha = 30$ cm^{-1}. This value is larger than typical values of AlGaInP-based laser diodes [6], [7]. We show below that the observed intensity distribution is a result of the contribution from the absorbing GaAs substrate.

IV. THEORETICAL CONSIDERATIONS

A. *Waveguide Dispersion*

To get insight into the interaction of waveguide dispersion, scattering, and material absorption, we performed some theoretical modeling. At first, an analytical model is presented that is

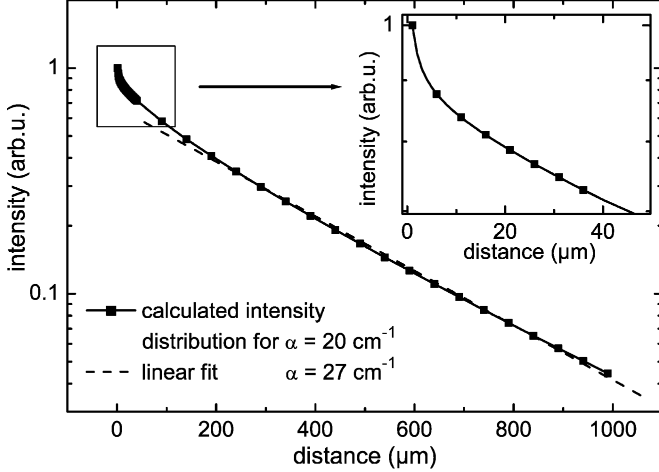

Fig. 5. Calculated intensity decay in a single-layer film on a substrate layer assuming no scattering ($\alpha = 20$ cm^{-1}, refractive index of film $n_f = 2.5$, and substrate $n_s = 1.75$). The width of the film a is 100 μm, and the height h is 2.5 μm. The waveguide dispersion increases the observed absorption; thus, a linear fit yields $\alpha = 27$ cm^{-1}. For small distances, the data is enlarged in the inset.

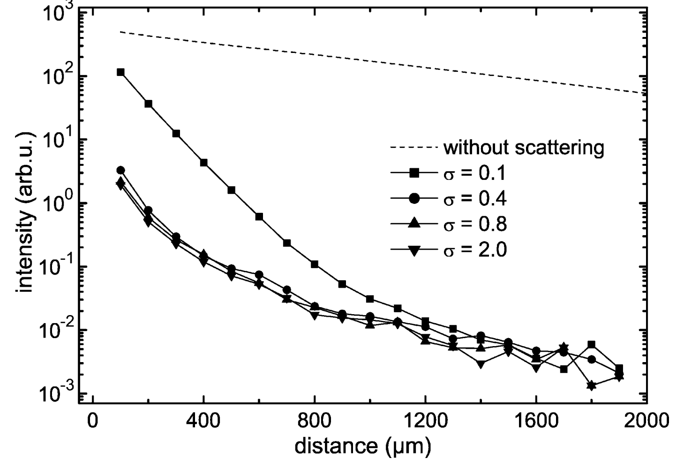

Fig. 6. Simulated intensity behavior with scattering using a Gaussian scattering distribution function. The width parameter σ has only little influence on the results ($\alpha = 7$ cm^{-1}).

used to study the consequences of waveguide dispersion on the intensity distribution. Since the complex layer structure of LEDs impedes a practical description, a simplified two-layer model consisting of a waveguide on top of a substrate is investigated. If no scattering is present, the intensity distribution can be calculated by an analytical ray-based transfer function $f(\theta, \phi, y)$ between emitter and detector. An isotropic emission of a point source and also an isotropic absorption behavior of the detector LED structure is assumed. Moreover, the physical size of the source has to be small compared with the propagation length. In this case, the calculation of subsequent incidence angles succeeds since all interfaces are perpendicular to each other. Thus, it is possible to describe the whole propagation process in terms of the initial ray direction θ and ϕ. Choosing the x axis as lateral direction and the y axis as propagation direction, the transfer function is (see Appendix I)

$$
\begin{aligned}
f(\theta, \phi, y) &= (r_{z,1} r_{z,2})^{\mu_z} (r_x)^{2\mu_x} \exp\left(-\frac{\alpha y}{\sin\theta \sin\phi}\right) \\
\mu_z &= \frac{y}{h \sin\phi \tan\theta} \\
\mu_x &= \frac{y}{w |\tan\phi|}.
\end{aligned}
\tag{1}
$$

$r_{z,1}(\theta)$ and $r_{z,2}(\theta)$ denote the reflection coefficients at the waveguide–air and waveguide–substrate interface, respectively, and $r_x(\theta, \phi)$ is the waveguide–air reflection coefficient in the lateral direction. It differs in its incident angle from $r_{z,1}$. The geometry is accounted for by the waveguide width w and the height h. The numbers of reflections in the z and x direction are μ_z and μ_x, respectively. α denotes the material absorption.

The waveguide dispersion effect enlarges the propagation distance, which is accounted by the exponential term in (1). Therefore, the observed intensity decay is larger than calculated by a pure exponential law and the associated waveguide length. Initially, no polarization is assumed; thus, 50% of the power is transverse electric (TE) and transverse magnetic (TM) polarized. The TE-polarized light with respect to the upper and lower interface is TMlike on the sidewalls, and vice versa. Each initial polarization is considered separately for the whole propagation. The photocurrent of the detector LED is obtained by integration of $f(\theta, \phi, y)$ with respect to θ and ϕ for each initial polarization and added up.

In a first example, we calculated the intensity distribution function for a nitride-based sample, which is illustrated in Fig. 5. Within the first 40 μm, losses from leaky modes dominate the intensity decay. Afterwards, the behavior is almost exponential. As expected, the observed intensity decay is larger than the material absorption caused by waveguide dispersion, which is accounted for by $\sin\theta \sin\phi$ in the exponential term in (1). However, after a short distance, the decay is almost exponential, and there the waveguide dispersion alone cannot explain the measured intensity distribution. Thus, further effects have to be taken into account.

B. Light Propagation in the Presence of a Dominating Scattering Effect

Nitride-based LEDs typically exhibit a large defect density in the buffer layer. Therefore, one possibility for the observed deviations might be scattering at the almost amorphous crystal structure at the interface between substrate and GaN layer. The presence of scattering yields additional optical losses in the waveguide since part of the light will be extracted. To study surface scattering, a ray tracer is employed. It calculates the complete trajectory for each ray and allows a summation of power at different distances to the emitter. Scattering is described by a statistical change in the propagation direction (see Appendix II). The scattered direction is calculated by a Gaussian distribution function with width σ centered about the specular ray for each reflection. A small σ causes a narrow scattering distribution and an almost undisturbed propagation. For the simulation, the same geometry and refractive indexes as those used for the undisturbed waveguide are taken. In Fig. 6, the obtained intensity distribution is depicted. The presence of scattering causes a bending of the intensity distribution curve with increasing σ. If σ is chosen between 0.4 and 2.0, the intensity behavior gets more and more independent from the absolute value of σ.

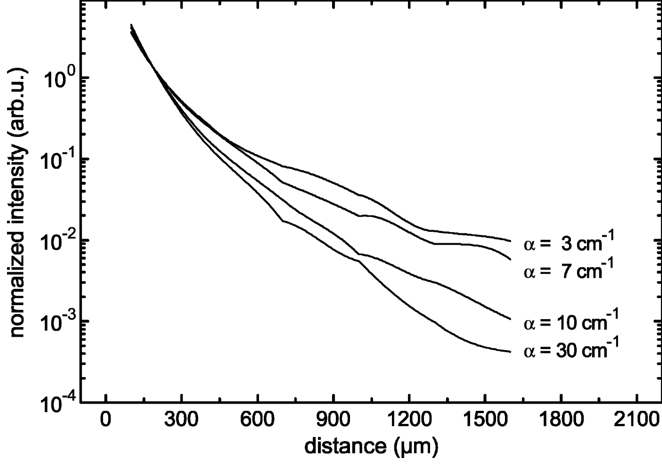

Fig. 7. Simulated intensity distribution for different absorption coefficients ($\sigma = 0.8$).

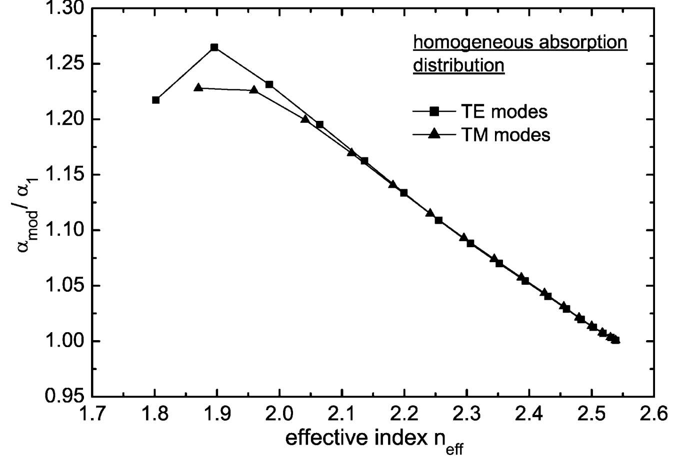

Fig. 8. Dependence of the modal absorption on the effective index of a homogeneous absorption distribution for the layer structure of Table I. It is found that the modal absorption normalized to the layer absorption α_1 for a given effective index does not depend on the layer absorption α_1 itself, which was varied in the range of 1–100 cm^{-1}. Thus, the modal absorption is proportional to the absorption α_1 for each n_{eff}.

In contrast, a strong dependence on the absorption coefficient remains (Fig. 7).

Surface scattering losses combined with the waveguide dispersion effect lead to mode-dependent absorption losses. A mode with a high effective index propagates in a nearly straight way through the waveguide without significant interaction with the surface. Modes with small effective indexes, on the other hand, will experience more surface reflections, leading to increased scattering losses. Thus, the modal losses depend strongly on the effective index. This dependence leads to the measured nonexponential intensity distributions. However, modal-dependent losses can also be the result of an inhomogeneous absorption distribution.

C. Light Propagation in the Presence of Inhomogeneous Absorption

The poor material quality at the substrate–GaN interface can lead to a significant band tail. Thus, we believe that the interface and part of the buffer layer can be regarded as a highly absorbing layer, and therefore, an inhomogeneous absorption distribution may be present. In this case, however, the dominant loss mechanism is absorption, not scattering.

For this model, we assume that no scattering is present in the structure. The solution of the electric field E_y of the Helmholtz equation is then independent of the propagation direction x and can be calculated based on the transfer matrix approach. A plane wave

$$E_y = \left(E_y^{(+)} \exp\{ik_z z\} + E_y^{(-)} \exp\{-ik_z z\}\right) \exp\{ik_x x\} \tag{2}$$

with complex k_z and k_x is a solution of the Helmholtz equation

$$\Delta E_y + k_0^2 E_y = 0. \tag{3}$$

The application of the boundary conditions leads to a finite number of modes with a complex effective refractive index

$$n_{\mathrm{eff}} = \frac{k_x}{k_0}. \tag{4}$$

k_0 denotes the vacuum wave vector. The imaginary part of the effective index contains the extinction from which the modal absorption is calculated.

In the following, we compare homogeneous and inhomogeneous absorption according to Tables I and II (see Fig. 1 for explanation of the abbreviations). We focus on the nitride samples containing a highly absorbing layer at the substrate–GaN-layer interface. The remaining layers of the structure are of high material quality and will thus show low absorption. For the AlGaInP-based samples, the highly absorbing GaAs substrate causes a similar effect at 650 nm.

For homogeneous absorption, one expects to observe the bare waveguide dispersion effect. The increase in path length should therefore depend only on the effective index and not on the value of the material absorption α_1. This behavior is found for absorption coefficients of $\alpha_1 = 1$ cm^{-1}, 10 cm^{-1}, and 100 cm^{-1}. Thus, a plot of $\alpha_{\mathrm{mod}}/\alpha_1$ results in the same curve (Fig. 8).

The situation is different for inhomogeneous absorption. In the following example, we assume an absorbing bottom layer with an absorption coefficient of $\alpha_2 = 3000$ cm^{-1} and a thickness $d_2 = 300$ nm in order to study the effect (see Fig. 9). The sinusoidal behavior of the absorption coefficient versus the refractive index is caused by the overlap of the mode profile with the absorbing layer. Moreover, for large refractive indexes, a sudden drop of the modal absorption is observed. For those modes, the penetration depth into the absorbing layer is weak.

The range of the obtainable modal absorption coefficients are much larger than for a homogeneous absorbing structure. It is shown subsequently that the intensity distribution obtained by PMM can only be described if such a large spreading in the modal absorption is present.

For the further application of the model, it is necessary to estimate suitable modal absorption coefficients to describe the intensity distribution. The asymptotic behavior of the intensity decay depicted in Fig. 3 can be used to determine the order of magnitude of the modal absorption.

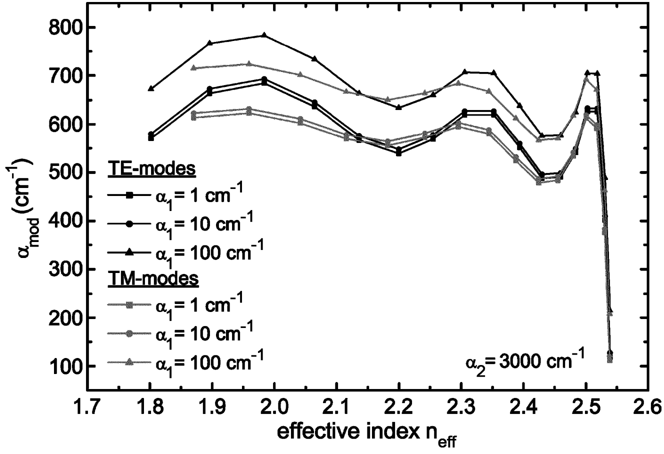

Fig. 9. Dependence of the modal absorption on the effective index of an inhomogeneous absorption distribution (layer structure of Table II). The sinusoidal behavior is due to the overlap of the mode profile with the absorbing layer. The linear dependence on the right-hand side can be explained by different penetration depths into the absorbing layer.

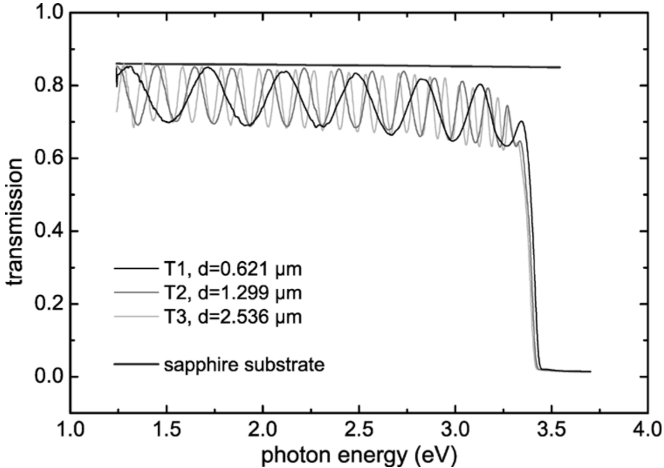

Fig. 10. Transmission curves for GaN on double-sided polished sapphire (samples T1–T3). As can be seen, the thickness does not influence the envelopes, and a significant difference in the region 2–3 eV to the sapphire transmission is observable.

Furthermore, the amount of absorbed power must be known. This cannot be calculated from the lateral measurement data; thus, an additional measurement by a different method is required. For this purpose, another series of samples has been investigated using both the transmission method and the photothermal deflection spectroscopy (PDS) [9]. Three samples T1, T2, and T3 have been investigated which consist only of a single GaN layer with different film thicknesses ranging from 0.62 to 2.53 μm grown on double-sided polished sapphire substrates. The obtained transmission curves are depicted in Fig. 10. For layers without absorption, the transmission should achieve the value of sapphire whenever the optical thickness of GaN is a multiple of $\lambda/2$. As can be seen in the range between 2.0 and 3.3 eV, the envelope transmission is noticeably reduced independently of the thickness. Thus, we conclude that the reduction is not caused by a bulk absorption but by a thin highly absorbing part of the layer. By numerical simulation of the transmission [9], only an amount of absorbed power (absorbance

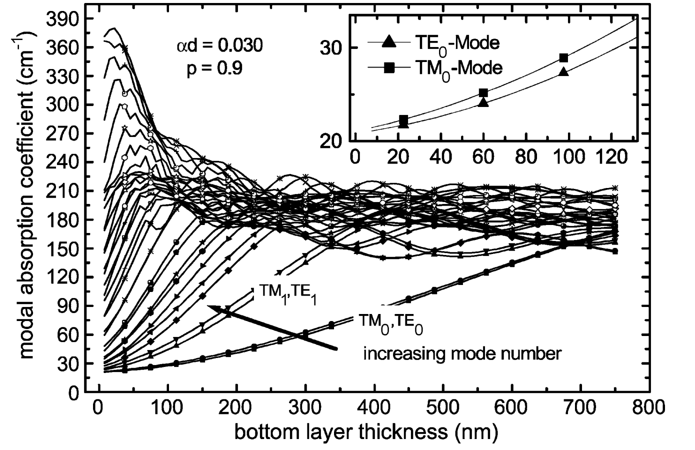

Fig. 11. Modal absorption coefficients versus bottom-layer thickness for $\alpha d = 0.030, p = 0.9$, and the layer structure of Table II. As can bee seen, the modal absorption spreads with decreasing bottom-layer thickness. (The inset depicts magnified curves with same units.)

value) $\alpha d = 0.030$ can be determined since neither the transmission measurement nor the PDS can be used to determine the absorbing-layer thickness. α denotes the absorption, and d the thickness of the absorbing layer.

In order to eliminate this ambiguity, we investigated which modes were necessary to describe the measured intensity distribution. Modes with a large absorption coefficient decay quickly and no longer show up in the observed range. Thus, only modes with slopes lying between the two tangents shown in Fig. 3 are of interest. The limiting absorption coefficients are $\alpha_{\min} = 10.5$ cm^{-1} and $\alpha_{\max} = 80.5$ cm^{-1}. The product αd can be distributed into the bottom layer d_1 and a remaining GaN layer d_2 according to

$$\alpha d = \alpha_1 d_1 + \alpha_2 d_2. \quad (5)$$

Besides the thickness degree of freedom, the relative composition of absorption can be changed. One possibility is

$$\alpha_2 d_2 = p \cdot \alpha d \quad (6)$$

with $0 \leq p \leq 1$. p denotes the relative absorbed power for normal incidence on the sample, which is the fraction of power absorbed in the bottom layer for the transmission measurement. Due to the overlap of the modal-field profile with the two layers, the values of d_1 and d_2 are important for the intensity decay of the PMM. Both parameters p and d_1 of the buffer layer have been varied for $\alpha d = 0.030$. In Fig. 11, the modal absorption coefficient versus buffer thickness is shown for a representative subset of modes. The absorbance distribution factor was set to $p = 0.9$. To get low absorption coefficients of about $\alpha_{\min}$, it is obviously necessary to have a thin absorbing bottom layer. The dependence of p is shown in Fig. 12 for the first six modes. As can be seen, the modal absorption coefficient drops below $\alpha_{\min}$ for a thickness of $d_{2,\max} = 130$ nm. This can be regarded as the maximum layer thickness since $\alpha_{\min}$ has been the minimal observed absorption of the lateral intensity decay. Finally, the intensity distribution can be described by

$$I = I_0 \sum b_i \exp\{-\alpha_i x\} \quad (7)$$

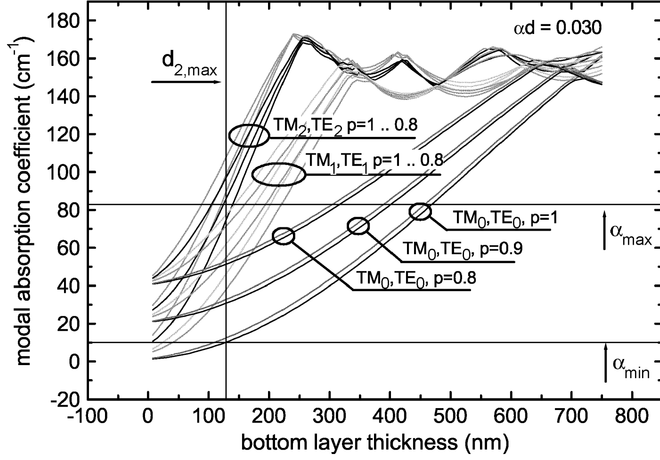

Fig. 12. Influence of the fraction of absorbed power p in the bottom layer on the first three TE and TM modes for the structure of Table II. Limits for the absorption coefficients are taken from Fig. 3. From $\alpha_{\min}$, the maximal thickness of the absorbing layer $d_{2,\max}$ can be estimated to be 130 nm.

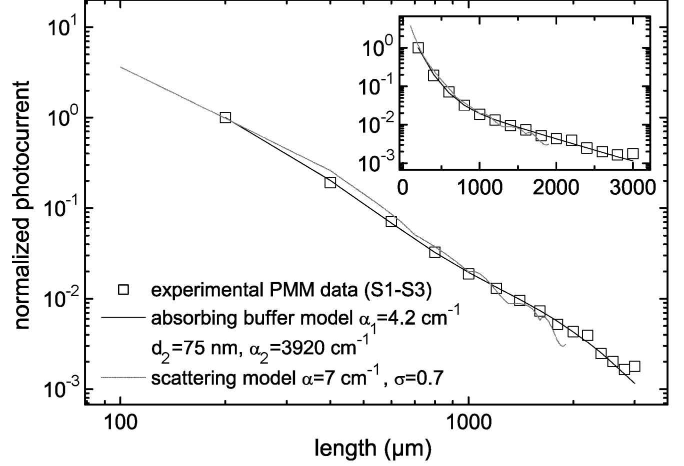

Fig. 13. Fit of the intensity distribution for InGaN-LED structures for both the scattering model and the absorbing-layer model. As can be seen, the absorbing-layer model fits much better to the experimental data. For comparison, the inset depicts the same data similar to Fig. 3.

where b_i denotes the modal excitation factor for the mode i, and α_i the corresponding modal absorption coefficient. x is the propagation distance. The theoretical modeling of the modal excitation factors is subject to further investigations; in this paper, we used them only as fitting parameters.

V. Results

A. InGaN-on-Sapphire-Based LED Structures

The two simulation models were utilized to fit the measurement data. The simulation model is fitted at the experimental measurement data according to (7) using the Levenberg–Marquardt algorithm. During the fit, the eigenmodes of the layer structure and thus the modal absorption coefficients have been calculated. Thus, besides the modal excitation factors b_i, the important parameters p and d_2 were the only fitting parameters. We observed a weak dependence on the modal excitation factors, but the fit was strongly influenced by the parameters p and d_2. This behavior results in a small error in d_2 and p and can be explained by an overlap effect of the mode profile with the absorbing layer. We obtained $d_2 = 75$ nm and $p = 0.98$. Using (5) and (6), the bottom-layer absorption $\alpha_2 \approx 3900$ cm^{-1} and the absorption of the remaining LED structure $\alpha_1 = 4$ cm^{-1} can be calculated.

When starting with the scattering model, the simulation curves fit the data best for an absorption coefficient of $\alpha = 7$ cm^{-1} and a scattering parameter $\sigma = 0.8$. While the scattering model describes the data fairly well (see inset of Fig. 13), a perfect agreement even in logarithmic scale and across three orders of magnitude is achieved for the absorbing-layer model (Fig. 13). Both models however, predict similar values for the absorption coefficient. Although either of them allows a correct extraction of the absorption coefficient from the measured intensity distribution, it should be emphasized that photothermal deflection spectroscopy measurements

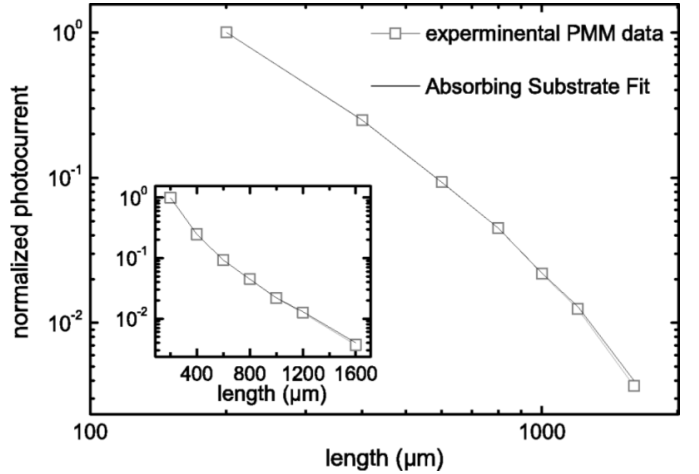

Fig. 14. Fit of the intensity distribution for AlGaInP-based LED structures based on the absorbing substrate model.

[9] clearly lead to the conclusion that the physical origin for the nonexponential decay is absorption and not scattering.

B. AlGaInP-Based LED Structures

For AlGaInP-based devices, the confinement of the optical waves is based on an absorbing substrate. This is very different from a dielectric waveguide; and therefore, the scattering model is not applicable. In contrast, the absorbing-layer model should by definition describe the experimental facts very well. In Fig. 14, a similar least-square fit, as in Fig. 13, is presented. As can be seen, the data is very well represented by the simulation curve. However, since the guidance is based on absorbance, no comparable interference effect exists. For a highly absorbing cladding layer, the modal absorption coefficients in AlGaInP-based devices increase continuously with decreasing effective index. Therefore, many more modes may contribute to the intensity distribution than for InGaN-based samples. No value for the material absorption coefficient can be calculated from the experimental data without further modeling of the mode excitation.

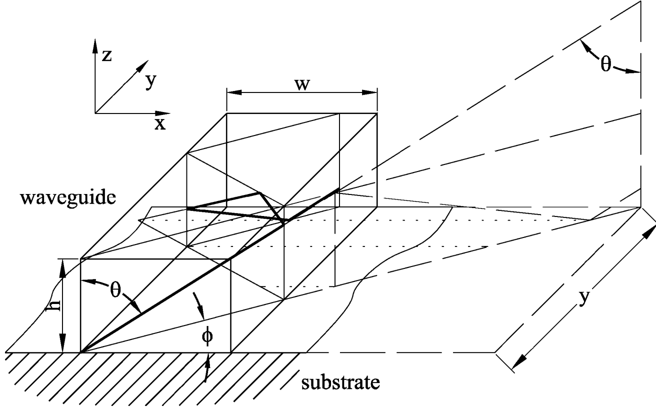

Fig. 15. Calculation of waveguide dispersion: A ray (solid dark line) propagating with azimuthal angle ϕ and polar angle θ in the waveguide is successively mirrored. An undisturbed ray propagation is obtained (prolonged dashed line). The effective propagation distance is $y(\sin\phi\sin\theta)^{-1}$.

VI. Conclusion

The lateral intensity distribution in InGaN-on-sapphire-based LEDs and AlGaInP-based LEDs has been investigated. The nitride-based samples exhibit a nonexponential intensity decay that is nearly independent of the emission wavelength of the investigated samples (404–433 nm). Likewise, the 650-nm-emitting AlGaInP sample shows a region where the behavior is strictly exponential. However, a similar nonexponential intensity decay is observed for short distances. Furthermore, a theoretical model is presented and the effect of waveguide dispersion and emission from leaky modes is studied. It is found that the emission from leaky modes is not the dominating factor for the observed intensity distribution. Especially for short propagation lengths, the dispersion effect leads to a curve of intensity versus distance, which decreases considerably faster than what is expected from Lambert–Beers law and the normal material absorption. Ray-tracing simulations reveal that scattering causes a nonexponential intensity decrease. However, in the presence of significant absorption, it is still possible to derive the absorption coefficient of laterally guided modes. Moreover, the nonexponential intensity distributions can only be obtained if modal-dependent absorption losses are present. For this reason, an absorption model is developed that introduces modal-dependent absorption losses based on the overlap of the mode profile with a highly absorbing layer close to the substrate and allows a much better representation of the experimental data. Surface scattering and the absorbing layer have a similar influence on the intensity distribution of propagating light. While the scattering model leads to an absorption coefficient of $\alpha = 7$ cm^{-1} for the high-quality GaN layer, the absorption model leads to 4 cm^{-1}. The modal losses in the scattering model is described by the scattering parameter $\sigma = 0.8$. For the absorbing-layer model, the losses are caused by a thin absorbing layer with a thickness of $d_2 = 75$ nm and an absorption coefficient $\alpha_2 \approx 3900$ cm^{-1}. The thickness d_2 is larger than the nucleation layer thickness of 40 nm. However, since part of the reduction of dislocation takes place in the beginning of the buffer layer, the larger thickness is reasonable. By photothermal deflection spectroscopy [9], one can clearly identify the detrimental effects of such a highly absorbing layer, which is most likely the reason for the nonexponential intensity decay.

The presented techniques allow the optimization of LEDs by identification of the dominant loss mechanism. The small thickness of the highly absorbing layer indicates a poor material quality of the nucleation layer and the lowest part of the GaN-buffer layer. Due to the large amount of absorption, this layer becomes one of the major optical loss mechanisms of InGaN-LEDs grown on sapphire. Since a reduction of the absorption coefficient increases the output power exponentially, a marked improvement of efficiency and output power should be achievable. This can be done by a removal of both substrate and absorbing layer.

Appendix I

If no scattering is present, the intensity distribution can be analytically calculated. The fraction of detectable power to emitted power is described by the transfer function that is deduced in the following. The x axis is chosen in the lateral direction, and it is assumed that the y axis is the propagation direction, as shown schematically in Fig. 15. At first, waveguide dispersion is considered. As depicted, the propagation path within the waveguide can be folded out of the waveguide into a straight propagation. The increase in propagation path is obtained by

$$y_{\text{eff}} = \frac{y}{\sin\theta\sin\phi}.$$

The number of intersections μ_z in the z direction is calculated by modulo of the propagation distance in z direction and the height h

$$\mu_z = \frac{y}{h\sin\phi\tan\theta}.$$

For the lateral direction, μ_x is

$$\mu_x = \frac{y}{w|\tan\phi|}$$

with width w. Furthermore, the effective reflection coefficient for the whole propagation r_{eff} is

$$r_{\text{eff}} = (r_{z,1}r_{z,2})^{\frac{\mu_z}{2}} r_x^{\mu_x}$$

where $r_{z,1}$ denotes the reflectivity at the waveguide–air interface in z direction, $r_{z,2}$ the reflectivity at the waveguide–substrate interface, and r_x the reflectivity at the waveguide–air interface in x direction. The square of r_{eff} is the intensity reflection coefficient R_{eff}.

$$R_{\text{eff}} = (r_{z,1}r_{z,2})^{\mu_z}(r_x)^{2\mu_x}.$$

Thus, the transfer function for one polarization is

$$\begin{aligned} f(\theta,\phi,y) &= (r_{z,1}r_{z,2})^{\mu_z}(r_x)^{2\mu_x}\exp\left(-\frac{\alpha y}{\sin\theta\sin\phi}\right) \\ \mu_z &= \frac{y}{h\sin\phi\tan\theta}, \\ \mu_x &= \frac{y}{w|\tan\phi|}. \end{aligned}$$

The photocurrent is obtained by numerical integration with respect to θ and ϕ, for both, initially, TE-like and TM-like modes.

Appendix II

If scattering is taken into account, a ray tracer is applied. For the simulation, a statistical description of surface scattering is used; the direction of the specular reflection is modified by a Gaussian distribution function. For that purpose, the direction cosines $l = \cos\alpha$ and $m = \cos\beta$ of the specular ray are calculated. The angle $\alpha(\beta)$ lies in between the x axis (y axis) and the specular ray direction of a local coordinate system. The scattering distribution function then modifies these values according to

$$f_{l,m}(l,m) = \frac{1}{\sigma\sqrt{2\pi}} \exp\left(-\frac{r^2}{2\sigma^2}\right)$$

where

$$\begin{aligned} l &= l_{\text{scattered}} - l_{\text{specular}} \\ m &= m_{\text{scattered}} - m_{\text{specular}} \\ r &= \sqrt{l^2 + m^2}. \end{aligned}$$

σ is the standard deviation of the rotationally symmetric Gaussian scattering distribution.

References

[1] M. Rattier, H. Benisty, R. P. Stanely, J. F. Carlin, R. Houdre, U. Oesterle, C. J. M. Smith, C. Weisbuch, and T. F. Krauss, "Toward ultrahigh-efficiency aluminum oxide microcavity light-emitting diodes: Guided mode extraction by photonic crystals," *IEEE J. Select. Topics Quantum Electron.*, vol. 8, pp. 238–247, Mar.–Apr. 2002.

[2] R. Windisch, C. Rooman, B. Dutta, A. Knoblauch, G. Borghs, G. M. Döhler, and P. Heremans, "Light-extraction mechanisms in high-efficiency surface-textured light-emitting diodes," *IEEE J. Select. Topics Quantum Electron.*, vol. 8, pp. 248–254, Mar.–Apr. 2002.

[3] F. A. Kish, F. M. Steranka, D. C. DeFevere, D. A. Vanderwater, K. G. Park, C. P. Kuo, T. D. Osentowski, M. J. Peanasky, J. G. Yu, R. M. Fletcher, D. A. Steigerwald, M. G. Craford, and V. M. Robbins, "Very high-efficiency semiconductor wafer-bonded transparent-substrate $(Al_xGa_{1-x})_{0.5}In_{0.5}P$/GaP light-emitting diodes," *Appl. Phys. Lett.*, vol. 64, no. 21, pp. 2839–2841, 1994.

[4] M. O. Holcomb, M. R. Krames, G. E. Hofler, C. Carter-Coman, E. Chen, P. Grillot, K. Park, N. F. Gardner, J.-W. Huang, J. Posselt, D. Collins, S. A. Stockman, G. M. Craford, F. A. Kish, I.-H. Tan, T. S. Tan, C. P. Kocot, and M. Hueschen, "High power truncated-inverted pyramid $(Al_xGa_{1-x})_{0.5}In_{0.5}P$ light-emitting diodes," in *Proc. SPIE*, vol. 3938, 2000, pp. 77–81.

[5] S. S. Schad, B. Neubert, M. Seyboth, F. Habel, C. Eichler, M. Scherer, P. Unger, W. Schmid, C. Karnutsch, and K. P. Streubel, "Absorption of guided modes in light emitting diodes," in *Proc. SPIE*, vol. 4996, 2003, pp. 10–17.

[6] M. Mannoh, J. Hoshina, S. Kamiyama, H. Ohta, Y. Ban, and K. Ohnaka, "High power and high-temperature operation of GaInp/AlGaInp strained multiple quantum well lasers," *Appl. Phys. Lett.*, pp. 1173–1175, 1993.

[7] H. D. Summers and P. Rees, "Experimental investigation of the differential gain in semiconductor lasers and its influence on Q-switching performance," *Appl. Phys. Lett.*, pp. 2009–2011, 1996.

[8] G. M. Laws, E. C. Larkins, I. Harrison, C. Molloy, and D. Somerford, "Improved refractive index formulas for the AlGaN and InGaN alloys," *J. Appl. Phys.*, vol. 89, no. 2, pp. 1108–1115, 2001.

[9] S. S. Schad, B. Neubert, J. Brüning, C. Eichler, F. Habel, F. Scholz, P. Unger, and D. Hofstetter, "Absorption in InGaN-on-sapphire LED-structures: Comparison between the photocurrent measurement method (PMM) and the photothermal deflection spectroscopy," in *Proc. SPIE, Light-Emitting Diodes: Research, Manufacturing, Applications*, vol. 5336, 2004, to be published.

Sven-Silvius Schad was born in Friedrichshafen, Germany, 1974. He received the Dipl.-Ing. degree in electrical engineering from the University of Ulm, Ulm, Germany, in 2000.

He became a Research Staff Member with the Department of Optoelectronics, University of Ulm. He is working on simulation and measurement of AlGaInP- and InGaN-based light-emitting diode devices.

Barbara Neubert was born in Neumünster, Germany, 1974. She received the Dipl.-Ing. degree from the University of Ulm, Ulm, Germany, in January 2002.

Since then she worked with the Department of Optoelectronics, University of Ulm, as a Research Staff Member. She develops device processing of red light-emitting diodes.

Christoph Eichler was born in Schwäbisch Hall, Germany, in 1974. He received the Dipl.-Ing. degree from the University of Ulm, Ulm, Germany, in 2001.

Since then he is a Research Staff Member at the Department of Optoelectronics, University of Ulm, where he is working on measurement and simulation of laser diodes.

Marcus Scherer was born in Augsburg, Germany, in 1974. He received the Dipl.-Ing. degree from the University of Ulm, Ulm, Germany, in 1999. He is currently working toward the Ph.D. degree at the same university.

He joined the Department of Optoelectronics, University of Ulm, in 1999 as a Member of the Research Staff. He is responsible for device processing and development of blue light-emitting diodes.

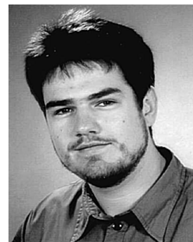

Frank Habel was born in Ulm, Germany, in 1975 and received the Diploma degree from the University of Ulm, Ulm, Germany, in 2001. He is currently working toward the Ph.D. degree at the same university.

His research involves metal–organic vapor phase epitaxy (MOVPE) and hybrid vapor phase epitaxy (HVPE) growth of GaN. His primary interest is the reduction of dislocation density in GaN layers grown on common substrates like sapphire.

Matthias Seyboth received the Dipl.Phys. degree from the University of Ulm, Ulm, Germany, in 1999. He is currently working toward the Ph.D. degree in electrical engineering with the Department of Optoelectronics, University of Ulm.

His research area is the growth of GaN-based electronic and optoelectronic structures by metal–organic vapor phase epitaxy (MOVPE).

Ferdinand Scholz was born on November 19, 1954. He received the Diploma in physics and the Ph.D. degree for studies on metal–organic vapor phase epitaxy (MOVPE) of GaInAs–InP quantum-well structures from the the University of Stuttgart, Stuttgart, Germany, in 1981 and 1986, respectively.

From 1986 to 2003, he was engaged as head of the epitaxial group of the 4 Physikalisches Institut of the University of Stuttgart in studies of liquid phase epitaxy and MOVPE of III–V compound semiconductors. In 1996, he was a Visiting Scientist at NTT Basic Research Laboratories, Atsugi, Japan. In 2003, he joined the Department of Optoelectronics, Ulm University, Ulm, Germany, as a Full Professor, where he is heading the GaN group. Main topics of his current research work include epitaxial growth and investigations of group III nitrides, quantum well, and optoelectronic device structures. Recent studies covered GaInP–AlGaInP for applications in high-power semiconductor lasers and vertical-cavity surface-emitting lasers emitting around 650 nm. He is currently involved in several national research projects about these topics. He has authored or coauthored more than 200 papers in refereed journals and holds two patents.

Dr. Scholz is a Member of the Deutsche Physikalische Gesellschaft (DPG) and the Deutsche Gesellschaft für Kristallwachstum und Kristallzüchtung (DGKK).

Daniel Hofstetter was born in Zug, Switzerland, in 1966. He received the diploma in physics from the Swiss Federal Institute of Technology (ETHZ), Zurich, Switzerland, in 1993 with a thesis on photoacoustic spectroscopy on fatty acid using gas lasers, and the Ph.D. degree from the Paul Scherrer Institute, Zurich, Switzerland, in 1996, for work that included the design, fabrication, and testing of a semiconductor-based monolithically integrated Michelson interferometer for optical displacement measurements.

After an apprenticeship as an Electrical Mechanic at Landis & Gyr, Zug, Switzerland, from 1982 to 1986, he became a Physics Technician. From 1996 to 1998, he was with the XEROX Palo Alto Research Center, Palo Alto, CA, developing single-mode violet-blue diode lasers in the InGaN–GaN material system. In 1998, he joined the group of Jerome Faist at the Physics Institute of the University of Neuchatel, Neuchatel, Switzerland, where his work focused on the fabrication and testing of high-performance distributed feedback quantum cascade lasers. Since 2002, he has been an Assistant Professor at the University of Neuchatel working on intersubband photodetectors both in the near- and the far-infrared wavelength range. He is currently also a Visiting Scientist at the Department of Optoelectronics of the University of Ulm, Ulm, Germany, and at the ECE Department of Cornell University, Ithaca, NY.

Peter Unger (M'98) was born in Aachen, Germany, on November 25, 1957. He received the Dipl.-Phys. degree and the Ph.D. degree in physics (with highest honors) from the Technical University of Aachen, Aachen, Germany, in 1985 and 1989, respectively.

In 1985, he joined the Institute of Semiconductor Electronics at the Technical University of Aachen, where he was involved in nanometer-scale electron-beam lithography, dry-etching techniques, and the fabrication technology of Fresnel zone plates for X-ray microscopy. From 1989 to 1994, he was a Research Staff Member at the IBM Zurich Research Laboratory, where he was working on the design and fabrication technology of semiconductor laser devices. Since 1994, he has been an Associate Professor at the Department of Optoelectronics of the University of Ulm, Ulm, Germany. His current research interests include high-power semiconductor laser devices and group III nitrides.

Dr. Unger is a Member of the German Physical Society.

Wolfgang Schmid was born in Pfaffenhausen, Germany, in 1969. He received the Dipl.-Ing. and Ph.D. degrees from the University of Ulm, Ulm, Germany, in 1996 and 2001, respectively.

He joined the Department of Optoelectronics, University of Ulm, in 1996 as a Member of the Research Staff. Since 2000, he has been a chip designer at OSRAM Opto Semiconductors, Regensburg, Germany.

Christian Karnutsch was born in Würzburg, Germany, in 1972. He received the Dipl.-Ing. degree in applied physics from the University of Applied Sciences, Heilbronn, Germany, in 1998 and the M.Sc. degree in photonics and optoelectronic devices from the Universities of St. Andrews and Edinburgh, U.K., in 2003. He is currently working toward the Ph.D. degree at the University Karlsruhe, Karlsruhe, Germany, where his dissertation work focuses on organic light-emitting diodes and lasers.

He was an Epitaxy Development Engineer at Osram OptoSemiconductors, Regensburg, Germany, from 1998 to 2002. During this time, he was working on AlGaInP-based light-emitting diodes and lasers. Since 2003, he has been with the Light Technology Institute, University Karlsruhe, Germany.

Klaus Streubel received the Ph.D. degree in physics from the University of Stuttgart, Stuttgart, Germany, in 1991.

He took a postdoctoral position at the Swedish Institute of Microelectronics, Stockholm, Sweden, in 1991. From 1993 to 1997, he was employed by the Royal Institute of Technology (KTH), Stockholm, Sweden, as a Research Staff Member. In 1997, he joined the Optoelectronics Department at Mitel Semiconductor AB, Järfälla, Sweden, where he was involved in compound semiconductor materials, III–V processing technology, and optoelectronic devices. His work included vertical-cavity lasers and resonant-cavity light-emitting diodes (LEDs) as well as micromachined optoelectronic components. In 1999, he joined the research and development group at Osram Opto Semiconductors, Regensburg, Germany. His interests now center on InGaAlP-based optoelectronic devices, such as LEDs and lasers. He has authored or coauthored more than 80 technical papers in international scientific journals and published some 95 conference papers.

Dr. Streubel is Member of the German Physical Society (DPG), the German Society for Crystal Growth (DGKK), and the IEEE Lasers & Electro-Optics Society (LEOS).